



SYSTEMS TECHNOLOGY, INC.

13766 Hawthorne Boulevard, Hawthorne, California 90250-7083, Phone (310) 679-2281, Fax (310) 644-3887

STI Paper No. 770

**Power Frequency: A Metric for Analyzing
Pilot-in-the-Loop Flying Tasks
(STI Paper Series)**

September-October 2012

**Amanda K. Lampton
David H. Klyde**

Published in
Journal of Guidance, Control, and Dynamics,
Vol. 35, No. 5, pp. 1526-1537, 2012



Power Frequency: A Metric for Analyzing Pilot-in-the-Loop Flying Tasks

Amanda Lampton* and David H. Klyde†
 Systems Technology, Inc., Hawthorne, CA 90250

DOI: 10.2514/1.55549

Crossover frequency is a parameter often used to characterize the pilot-vehicle system behavior for continuous control tasks with known forcing functions. However, for many tasks, such an input is not known, and in these cases cutoff frequency can be applied. While cutoff frequency is a useful parameter, it does not necessarily reflect pilot effort. Power frequency, derived from cutoff frequency via wavelet analysis, is introduced herein as a parameter that relates the frequency of pilot input with the intensity of that input. Scalogram-based time-varying counterparts to both the cutoff frequency and power frequency show how this relationship evolves through a given task. Both the cutoff and the power frequency are calculated for flight test data from an offset approach and landing task. The pilot ratings recorded for each evaluation are then compared to both the cutoff frequency and power frequency to determine if a correlation exists. Results show that there is significant scatter in the ratings versus cutoff frequency data and a strong correlation between ratings versus pilot input power frequency.

Nomenclature

dt	=	time interval
F_s	=	stick force
$F_{as,m}$	=	lateral stick force
$G_{\delta\delta}$	=	power spectral density
p	=	roll rate
t	=	time
T	=	total time
Y_c	=	controlled element
Y_p	=	pilot describing function

Greek

β	=	sideslip
δ_a	=	aileron position
δ_{a_l}	=	aileron position limited position
δ_{ac}	=	aileron position command
$\delta_{ac_{rl}}$	=	rate limited aileron position command
δ_c	=	surface command
δ_s	=	stick position
ϕ	=	roll attitude
τ_e	=	effective system time delay
ω	=	frequency
ω_c	=	crossover frequency
ω_{cutoff}	=	cutoff frequency
ω_G	=	power frequency
Ψ	=	integral of the power spectral density

Abbreviations

EP	=	evaluation pilot
FFT	=	fast fourier transform
FREDA	=	frequency domain analysis
PIO	=	pilot induced oscillation

PSD	=	power spectral density
RMS	=	root mean square
SP	=	safety pilot
STI	=	Systems Technology, Inc.
VSS	=	variable stability system

I. Introduction

PILOT ratings in the form of Cooper-Harper Handling Qualities Ratings [1] and Pilot-Induced Oscillation Tendency Ratings [2] are the most common source of data from a piloted simulation or flight test program involving the assessment of aircraft handling qualities. Accurate assessments can be obtained when the ratings are generated by experienced test pilots that are performing evaluation tasks with well-defined desired and adequate performance requirements. Still the pilot ratings represent a qualitative assessment, so there remains a need to quantify the results as well. To this end, numerous fixed and rotary wing metrics and criteria have been defined in military specifications [3,4] and elsewhere in the literature [5,6].

In addition to these standard handling qualities assessments based on qualitative pilot ratings and quantitative metrics and criteria, there is a desire to better understand the pilot-vehicle system as it relates to handling qualities assessments as well. To this end, a variety of pilot-vehicle system behavior models have been developed primarily as a means to describe the human pilot as he or she attempts to control the aircraft. For those scenarios in which the pilot attempts to compensate for a displayed error in a continuous control task, McRuer's Law or the crossover model applies [7]. The crossover model is valid for single-loop compensatory control (e.g., precision tracking). A block diagram for the compensatory control scenario is shown in Fig. 1. Here, the pilot controls the system output, m , in response to the displayed pilot-vehicle system error, e .

In short, the crossover model states that the pilot adjusts his/her characteristics such that the pilot-vehicle system can be represented by the following open loop transfer characteristics:

$$Y_p(j\omega)Y_c(j\omega) = \frac{\omega_c e^{-j\omega\tau_e}}{j\omega} = \frac{m}{e} \quad (1)$$

In the above equation and figure, Y_p is the pilot describing function, Y_c is the controlled element, ω_c is the crossover frequency, and τ_e is the effective system time delay. The key variables, ω_c and τ_e , are functions of pilot behavior, controlled element dynamics (airplane model), mission task variables, and environment (system delays, field-of-view, etc.). The crossover frequency is defined as the frequency on a Bode plot at which the pilot-vehicle system open-loop

Presented as Paper 2011-6539 at the AIAA Atmospheric Flight Mechanics Conference, Portland, OR, August 8–11, 2011; received 7 July 2011; revision received 13 March 2012; accepted for publication 13 March 2012. Copyright © 2012 by Amanda Lampton and Dave Klyde of Systems Technology, Inc. Published by the American Institute of Aeronautics and Astronautics, Inc., with permission. Copies of this paper may be made for personal or internal use, on condition that the copier pay the \$10.00 per-copy fee to the Copyright Clearance Center, Inc., 222 Rosewood Drive, Danvers, MA 01923; include the code 0731-5090/12 and \$10.00 in correspondence with the CCC.

*Staff Engineer, Research, Member AIAA; alampton@systemstech.com.

†Technical Director & Principal Research Engineer, Associate Fellow AIAA; dklyde@systemstech.com.

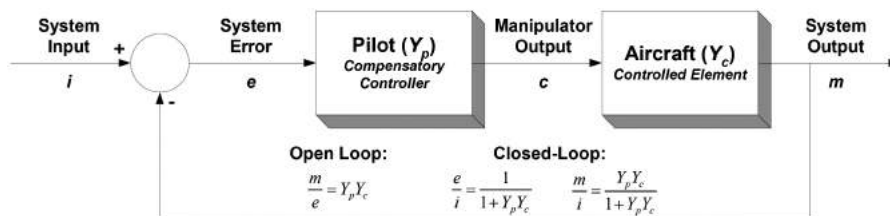


Fig. 1 Compensatory control scenario.

describing function amplitude ratio crosses the 0 dB line. It has been demonstrated through extensive research that those controlled elements that are most “k/s-like” in the region of crossover require the least compensation by the pilot. In turn, as pilot compensation increases and/or controlled element dynamics degrade, the achieved crossover frequency typically decreases.

The effective system time delay is a function of fundamental pilot latencies, the high frequency flight control system and aircraft dynamics (e.g., actuators, structural filters, structural modes, etc.), and added incremental time delays due to pilot compensation. Once again, the more “k/s-like” the controlled element is in the region of crossover, the less pilot compensation will be required and the smaller the effective time delay. When little or no compensation is required by the pilot and the higher frequency dynamics are negligible, the effective time delay will consist solely of the delay in the pilot’s response.

For those scenarios where the input is a known forcing function, key pilot-vehicle system parameters such as crossover frequency can be measured directly. In most common piloted simulation and flight test evaluation tasks, however, the input is not known. For these cases, a pilot cutoff frequency is defined [8]. As described later, the cutoff frequency uses a power spectral density of the pilot’s input to provide an estimate of crossover frequency. While cutoff frequency is a useful parameter, alone it does not seem to capture pilot workload. That is, it can provide a measure of the frequency of pilot activity, but not the level of that activity. Some efforts have been made to address this by comparing cutoff frequency, amplitude of pilot input, and handling qualities ratings in [9]. In this paper, a new metric, power frequency, is defined that combines these into a single parameter in an effort to provide a better correlation of the frequency of pilot input with the intensity of that input.

This paper begins with a description of the flight data used in the analysis of the power frequency in Sec. II. It describes the offset approach and landing task and the general format of the Smart-Cue/Smart-Gain concept that was the focus of the flight test. Section III defines the cutoff frequency as developed by Tischler and Remple [8] and the scalogram-based time-varying version. The next section, Sec. IV, derives the power frequency and time-varying power frequency from the cutoff frequency. The full analysis of the power frequency is discussed in Sec. V. This section includes details of flight test configurations, state time histories, input and output scalograms, time-varying cutoff and power frequency, and the relationship of the input and output maximum and average cutoff and power frequency to pilot handling qualities ratings.

II. Flight Test Data

The flight test data used herein is a product of a two phase study conducted by Systems Technology, Inc. (STI) and sponsored by NASA Dryden Flight Research Center that investigated the use of dynamic distortion to predict and alleviate loss of control. Flight testing of a precision offset landing task using the Calspan Learjet in-flight simulator was conducted in November 2006 and January 2007. Three test pilots participated in the flight tests; the data from two of these pilots is used to develop and test the power frequency. Pilot 1 is a Navy Test Pilot School (TPS) graduate who primarily flew fighter aircraft and can be classified as a high gain pilot. Pilot 2 is also a TPS graduate who flew primarily fighter aircraft and can be classified as a “golden arm,” meaning he is skilled at adjusting his gain and compensation to approach but not go over a “flying qualities cliff.”

The following subsections briefly describe the flight test platform, aircraft configuration, task, and the Smart-Cue/Smart-Gain.

A. In-Flight Simulator Description

The flight tests were conducted with a Calspan Corporation variable stability in-flight simulator, which for these tests was the modified Learjet Model-25 aircraft shown in Fig. 2 with a centerstick. The three modified Learjets provide three degree-of-freedom (3-DOF) in-flight simulation capabilities for advanced stability, control, and flying qualities demonstrations and research [10]. They are also used to test/demonstrate advanced flight control systems concepts. The three aircraft are used in these capacities to support flight test training of test pilots and flight test engineers around the world, as well as support new aircraft development programs.

The right seats of the Learjets have been extensively modified to serve as the Evaluation Pilot (EP) crew station. The normal Learjet wheel/column has been removed. It is replaced with one of three experimental controllers; 1) centerstick, 2) sidestick, and 3) wheel/column. Each of these two axis control inceptors has programmable variable feel capability, allowing simulation and evaluation of a wide range of characteristics. The Learjet’s aircraft rudder pedals have also been replaced with variable feel capability. Electrohydraulic servo actuators drive the aircraft’s primary control surfaces in response to pilot inputs and the signals from the Variable Stability System (VSS). The Safety Pilot (SP), whose controllers remain mechanically connected to the Learjet control surfaces, via cables, occupies the left seat.

B. Flight Control System Description

The feel system of the Learjets can be tailored to satisfy flight test requirements and to provide the proprioceptive feedback of interest. The key feel system elements are shown in the Fig. 3 block diagram. These include the dynamic characteristics of the Calspan control loader and the control system gearing. A summary of the baseline feel system characteristics for the lateral axis is listed in Table 1.

The key lateral axis control system elements downstream of the feel system are identified in Fig. 4. These elements include the software rate limiter, surface actuator, and surface position limits. The software rate limiter is the key dynamic distortion inducing element that was used in the flight test evaluation of Smart-Cue/Smart-Gain, which will be briefly outlined in Sec. II.D. The control surface actuator dynamics and surface position limits replicate those



Fig. 2 Variable stability Learjet 25 (Calspan photo).

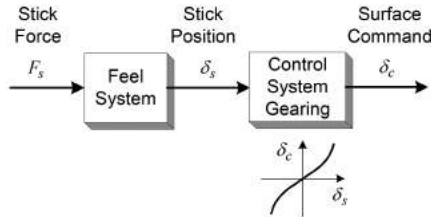


Fig. 3 Feel system elements.

found on the Calspan variable stability Learjet. Parameters for the control system elements are defined in Table 2.

C. Precision Offset Landing Task

The flight test data to be evaluated is for a precision offset landing task whose purpose was to evaluate dynamic distortion in the lateral axis. The nominal approach speed was 140 knots with gear down and flaps set to 20 deg, which is within normal operating conditions for this aircraft. The lateral-directional powered approach configuration is identified as the baseline roll cruise configuration with characteristics similar to a nominal Learjet 25 in which the configuration is susceptible to pilot-induced oscillations (PIO) in the presence of significant rate limiting. The roll rate to lateral stick force transfer function[‡] that represents this configuration is

$$\frac{p}{Fas_m} = \frac{4.0862e6(0)[0.335, 1.103]}{(-5.49e - 3)[0.249, 1.25](1.324)[0.7, 20][0.7, 44]} e^{-0.125s} \quad (2)$$

The offset landing task consists of a visual approach during which the evaluation pilot aligns the aircraft approximately 300 ft off the runway centerline (see Fig. 5). At 150 to 200 ft above the ground, the pilot corrects the offset to align with the centerline and attempts to touchdown within the desired parameters. The decision to correct is made by the SP. Offsets to the left or right can be used interchangeably; however, the direction of offset may often be dictated by the desire to turn away from civilian aircraft waiting in the hold short area. Typically, offsets were made to the right to take advantage of local visual cues. Each landing is treated as a “must land” situation in order to ensure a high pilot gain.

Desired performance requirements were to maintain approach airspeed within ± 5 kt, touchdown within 5 ft of the centerline and within ± 250 ft of the aimpoint, maintain a smooth sink-rate and touchdown, and no PIO. Adequate performance requirements were to maintain approach airspeed within -5 kt and $+10$ kt, touchdown within 25 ft of the centerline and within ± 500 of the aimpoint, and no PIO.

During a typical landing pattern evaluation, the SP configures the aircraft for landing, selecting the proper flight control experiment, and engaging the VSS while on downwind. The EP begins the evaluation on base turn and lines up on final for the offset landing. The EP initiates the offset correction on his own or based on radar altitude calls from the safety pilot. A precise flared landing is attempted using the instrument landing markers as the desired touchdown point. These markers are located 1000 ft from the threshold. Upon touchdown, the safety pilot takes control of the airplane and performs the takeoff and turns to downwind, while the evaluation pilot provides comments and handling qualities ratings for that configuration.

D. Smart-Cue/Smart-Gain

The heart of the Smart-Cue concept is to restore a force feedback cue similar to the ideal valve-bottoming characteristics in a fly-by-wire system configuration in the presence of distortions in the actual systems in an effort to reduce the occurrence and severity of PIO [12]. When the control surface position error, the difference between the commanded surface position and the actual surface position, deviates

sufficiently from the idealized manual control system, then Smart-Cue in the form of cuing and corrective forces are presented to the pilot. The cuing alerts the pilot to the presence of dynamic distortion caused by such issues as rate limiting. Two types of cuing forces form Smart-Cue and were evaluated in flight test—a gradient force and a friction force. The Smart-Cue gradient force is a restraining force that effectively increases the stick force gradient, and the Smart-Cue friction force is a restraining force that effectively acts as a coulomb friction force that is a function of the sine of the stick velocity. The final component investigated in flight test was the Smart-Gain, which uses position error as a metric to reduce command path gain as a means of avoiding loss of control [13]. Though testing the Smart-Cue/Smart-Gain concept was the main reason for conducting the flight tests, for the purposes of the development of the power frequency metric, it can be viewed as simply differences in the plant characteristics.

III. Cutoff Frequency

The cutoff frequency [8,14] is a spectral analysis method for determining the pilot operating frequency for pilot-in-the-loop flying tasks. It is an alternative measure when it is not possible to determine pilot-vehicle crossover frequency [15] directly. Cutoff frequency is a quantitative measure of pilot stick activity calculated by examining controller input power versus frequency. Specifically, the cutoff frequency is defined as the frequency at which the integral of the power spectral density (PSD) from $\omega = 0$ to ∞ is half of its total value. This is determined by calculating the ratio of root mean square (RMS) values expressed as $\Psi_1/\Psi_{\text{total}}$. Ψ_{total} is calculated by the integral:

$$\Psi_{\text{total}}^2 = \frac{1}{2\pi} \int_0^{\infty} G_{\delta\delta} d\omega \quad (3)$$

where $G_{\delta\delta}$ is the PSD function for the controller. Essentially, the mean square value is proportional to the area under the PSD curve. Similarly, Ψ_1 is calculated by the integral

$$\Psi_1^2 = \frac{1}{2\pi} \int_0^{\omega_1} G_{\delta\delta} d\omega \quad (4)$$

where Ψ_1 is the RMS value of the stick input signal (or rate output signal) over the frequency range $\omega = 0$ to ω_1 . Since the cutoff frequency is the frequency at the half power point, ω_{cutoff} is thus the frequency at which $\Psi_{\text{cutoff}}^2/\Psi_{\text{total}}^2 = 0.5$ or $\Psi_{\text{cutoff}}/\Psi_{\text{total}} = 0.707$, where $\omega_1 = \omega_{\text{cutoff}}$.

A. Calculating Cutoff Frequency

STI's FREQUENCY Domain Analysis software or FREDA is a Fast Fourier Transform (FFT) routine that is used to identify dynamic systems from flight test and simulation data [16]. In the process of identifying the system, the input PSD, output PSD, and remnant are calculated versus frequency to characterize the entire time history. To calculate the cutoff frequency, the pilot control inceptor input PSD calculated by FREDA is used. A similar measure can be attained using the aircraft output PSD. The PSD of choice is then numerically integrated and the frequency associated with the half power determined. FREDA is an in-house STI tool used in this analysis, but

Table 1 Lateral axis baseline feel system characteristics

Parameter	Roll
Spring gradient (lb/in)	5.65
Damping (lb · s/in)	0.395
Natural frequency (rad/s)	20
Damping ratio	0.7
Inertia (lb · s ² /in)	0.0141
Breakout (lbs)	0.25
Travel (in)	± 3.1
Control system gearing (deg/in)	-12.3

[‡]Shorthand notation: $a(s + b)[s^2 + 2\zeta\omega s + \omega^2] = a(b)[\zeta, \omega]$

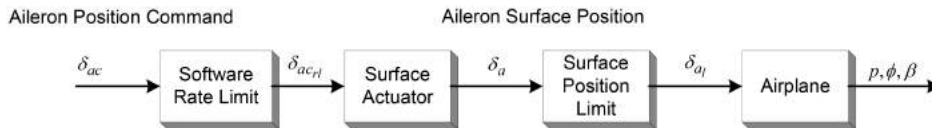


Fig. 4 Lateral axis control system elements.

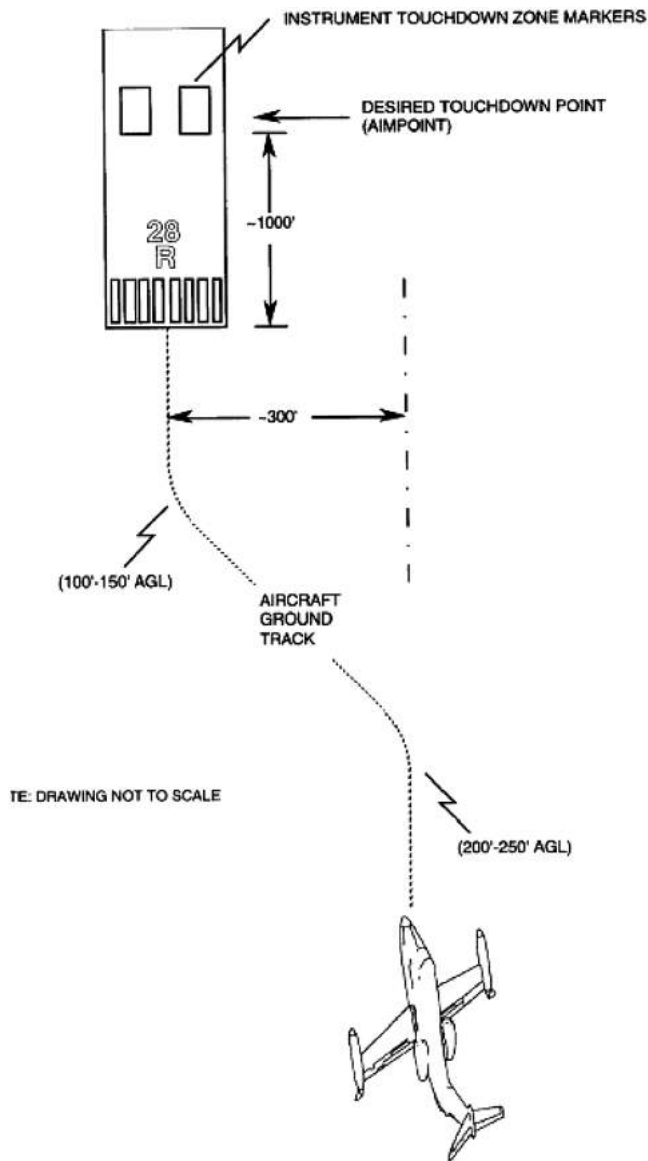


Fig. 5 Calspan offset approach (Ref. [11]).

is not the only option. Any system identification tool that can generate PSDs can be used to calculate the cutoff frequency.

B. Calculating Cutoff Frequency as a Function of Time

Wavelet transforms are a relatively new way to characterize time-varying systems. Rather than just a power versus frequency relationship averaged over the entire time history, the use of wavelet transforms can produce plots of power versus both time and frequency, as shown in Fig. 6. A particular class of this is called scalograms, which are used extensively by STI. In addition, unlike the windowed Fourier transform, the wavelet transform time window decreases as the frequency increases capturing more of the transient details at higher frequencies than the Fourier transform [17].

Intuitively, it is logical to assume that a pilot will change his/her control input behavior as a task progresses. The pilot becomes more comfortable flying the task, the pilot has performed the task more than once, the pilot is tuning his/her own response, the pilot becomes distracted or distressed, etc., all of which contribute to a time-varying change in input and output power. Furthermore, the pilot may be adapting to changing dynamics in the vehicle.

The cutoff frequency can then be calculated in a way similar to that described above. As stated, a scalogram shows the relationship between power, time, and frequency. Calculating the cutoff frequency entails integrating the power over the frequency range, so the time-varying cutoff frequency, $\omega_{cutoff}(t_i)$, can be calculated by numerically integrating the power over the frequency range for each time instant of the scalogram.

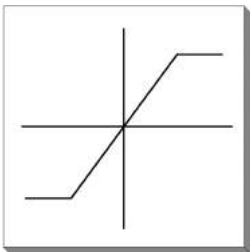
$$\frac{\Psi_i^2(t_i)}{\Psi_{total}^2(t_i)} = \frac{\frac{1}{2\pi} \int_0^{\omega_1(t_i)} G_{\delta\delta}(t_i) d\omega}{\frac{1}{2\pi} \int_0^{\infty} G_{\delta\delta}(t_i) d\omega} = 0.5 \quad (5)$$

where t_i is time instant i , $i = 1, 2, \dots, T/dt$, T is total time, and dt is the time interval.

IV. Power Frequency as a Function of Time

A detail that is lacking in the time-varying cutoff frequency is that even though it is calculated using the power at a given time instant, the magnitude of the power at that time relative to power at all other times is lost. This can result in a range of behavior in the time-varying cutoff frequency including a nearly uniform parameter over time or a parameter that has a number of large spikes at several points in time. The problem arises when these are compared to their associated scalograms. Time slices of the scalogram that show little activity and time slices with extreme activity could have similar cutoff frequencies simply due to the nature of the cutoff frequency equation.

Table 2 Lateral axis flight control system parameters

Flight control system element	Form	Parameter values
Software rate limit (deg/s)		$V_L = 30$ (Rate limited) $V_L = 150$ (Baseline)
Surface actuator	$\frac{\omega_n^2}{s^2 + 2\zeta\omega_n s + \omega_n^2}$	$\omega_n = 44$ rad/s; $\zeta = 0.7$
Surface position limits	$\delta_{a_{max}}$	± 40 deg

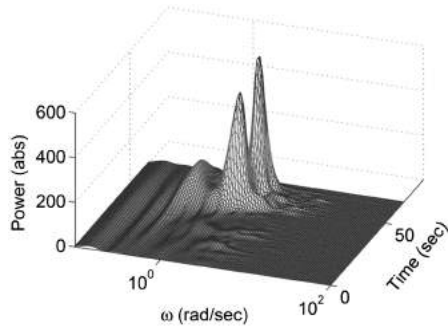


Fig. 6 Example scalogram.

To alleviate this issue, a new metric is defined, the power frequency $\omega_G(t_i)$, by introducing power back into the time-varying cutoff frequency. This is accomplished by simply multiplying the cutoff frequency at time, t_i , by the maximum of the PSD, $\max G_{\delta\delta}(t_i)$, over the frequency range, ω , at time, t_i . The metric is then scaled by dividing by 1000, an arbitrary term that is used to scale the parameter for the given problem. Thus the metric takes the following form,

$$\omega_G(t_i) = \frac{\omega_{\text{cutoff}}(t_i) \max G_{\delta\delta}(t_i)}{1000} \quad (6)$$

Multiplying the cutoff frequency by the maximum power effectively modulates the cutoff frequency and reflects the pilot or vehicle activity evidenced by the scalogram. When very little is happening in the pilot-vehicle system at a particular time instant, the time-varying cutoff frequency is tempered and reduced. When there is much activity indicated by spikes in the scalogram, the power frequency reflects that as well.

Power frequency can also be calculated as a single value for the entire time series using the cutoff frequency and PSD from FREDa or other system identification tool of choice. The same equation as that listed above for time-varying power frequency may be used without the time dependence.

V. Analysis

A. Representative Flight Tests

The flight test data analyzed here are the result of flight tests conducted to evaluate the Smart-Cue/Smart-Gain system. The data for two pilots, Pilot 1 and Pilot 2, are considered. Each pilot flew the approach and landing task several times with various Smart-Cue/Smart-Gain configurations in similar weather conditions and evaluated them by providing Handling Qualities Ratings (HQR) and Pilot Induced Oscillation Ratings (PIOR) for each configuration. The flight logs listing Smart-Cue/Smart-Gain configurations for Pilot 1 and Pilot 2 are listed in Tables 3 and 4, respectively.

To illustrate the utility of the power frequency, six example cases were selected from the available run sets listed in Tables 3 and 4. These include runs 04, 05, and 14 for Pilot 1 and runs 12, 13, and 18 for Pilot 2, which represent runs for each pilot in the baseline

aircraft, the aircraft with control surface rate limiting, and the aircraft with control surface rate limiting and Smart-Cue/Smart Gain, respectively.

B. Time Histories

The time histories consisting of lateral stick position and roll attitude angle for each of the example cases are shown in Fig. 7. These time histories illustrate the distinctions between the various runs. The roll attitude angle for the baseline aircraft and the aircraft with cuing appear similar with sharp changes when the evaluation pilot returns the aircraft to wings level flight. The magnitude of the stick input for these two cases for both pilots are generally the same for the majority of the maneuver. The main difference appears during the return to wings level flight where the magnitude of input for the rate limited without cuing case is 50% greater than that for the baseline case. The roll attitude angle from Run 05 for Pilot 1 shows PIO, which is reflected in lateral stick position as the pilot attempts to correct the oscillations of the rate limited aircraft. Run 13 for Pilot 2 shows PIO 50 s into the run as well. In both cases the safety pilot took over control of the aircraft.

C. Scalograms

Input and output scalograms for the six example cases are shown in Figs. 8–10. Plot scales are constant for ease of comparison.

The baseline cases for the pilots illustrated in Fig. 8 shows minimal activity through the majority of the run. There is a gentle increase in stick activity culminating in a peak around 0.8 rad/s near the 50 s mark for both pilots that corresponds to the roll attitude correction segment of the offset approach task. There is a similar peak in the roll rate scalogram that reflects the vehicle response to the pilot input.

In addition to showing the changes in input and output power, the scalograms also reflect differences between the pilots. The input power of Pilot 1 is focused mainly at that low frequency with a minor secondary peak at 1.06 rad/s. Pilot 2 evinces more activity in the higher frequency range throughout the run as shown by the ripples in the scalogram and the lower magnitude of the primary peak as compared to Pilot 1. These characteristics will be reflected in the time-varying cutoff and power frequencies.

Figure 9 shows the scalograms for the rate-limited aircraft for each pilot. Similar to the baseline case, there is little activity in the early stages of the maneuver as the pilot slowly changes roll attitude angle. However, the peaks resulting from the abrupt input to correct the roll attitude and line up for landing is much more pronounced for this case. Not only are the magnitudes of the primary peaks greater, they also appear at higher frequencies on the order of 1.15 rad/s with secondary peaks at 0.6 rad/s. The differences between the pilots are also less pronounced. The very evident difference in magnitudes is still present, but the scalograms for Pilot 1 are much smoother with most of the activity focused at the frequency of the peaks. This difference in magnitude and change in frequency between the baseline and rate-limited aircraft shows the impact of the rate-limited case. Both pilots battle with the aircraft by increasing input frequency and magnitude to achieve the task at hand.

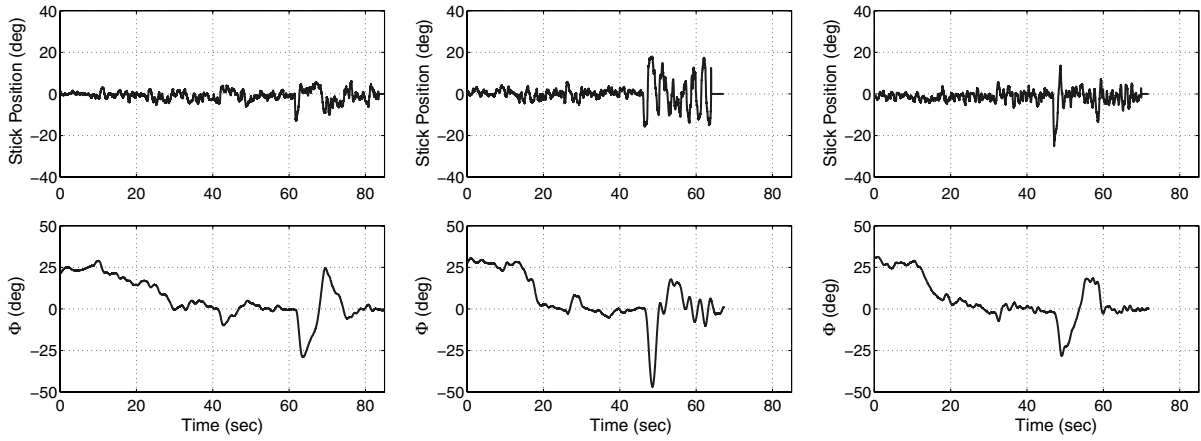
The scalograms for the rate-limited aircraft with cuing are displayed in Fig. 10. As with the previous cases, there is little activity

Table 3 Run log for pilot 1

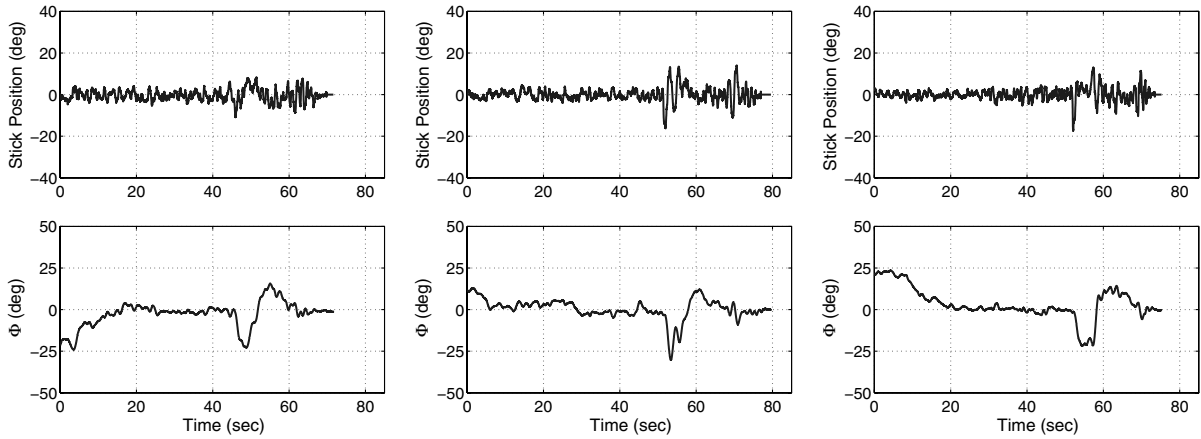
Run	Rate limit	Cue?	Gain	Friction	Gradient
04	None	No	-	-	-
05	30	No	-	-	-
06	30	Yes	✓	-	-
07	30	Yes	✓	-	-
08	30	Yes	✓	-	-
09	30	Yes	✓	✓	-
10	30	Yes	✓	✓	-
11	30	Yes	✓	✓	✓
12	30	Yes	✓	✓	✓
13	30	Yes	✓	✓	-
14	30	Yes	✓	✓	✓

Table 4 Run log for pilot 2

Run	Rate limit	Cue?	Gain	Friction	Gradient
12	None	No	-	-	-
13	30	No	-	-	-
14	30	Yes	✓	-	-
15	30	Yes	✓	✓	-
16	30	Yes	✓	✓	-
17	30	Yes	✓	✓	✓
18	30	Yes	✓	✓	✓
19	30	No	-	-	-

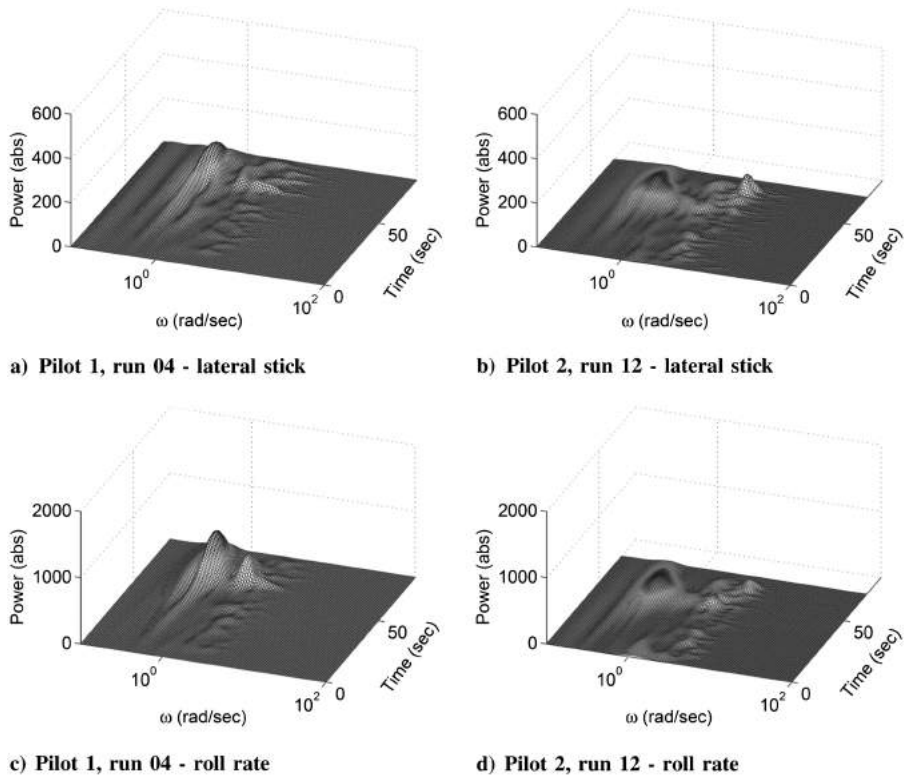


a) Pilot 1, run 04 - baseline aircraft b) Pilot 1, run 05 - rate limited aircraft c) Pilot 1, run 14 - rate limited aircraft with cuing



d) Pilot 2, run 12 - baseline aircraft e) Pilot 2, run 13 - rate limited aircraft f) Pilot 2, run 18 - rate limited aircraft with cuing

Fig. 7 Time histories.



a) Pilot 1, run 04 - lateral stick b) Pilot 2, run 12 - lateral stick
c) Pilot 1, run 04 - roll rate d) Pilot 2, run 12 - roll rate

Fig. 8 Scalograms for pilot input and output in baseline aircraft.

Downloaded by David Klyde on January 15, 2020 | http://arc.aiaa.org | DOI: 10.2514/1.55549

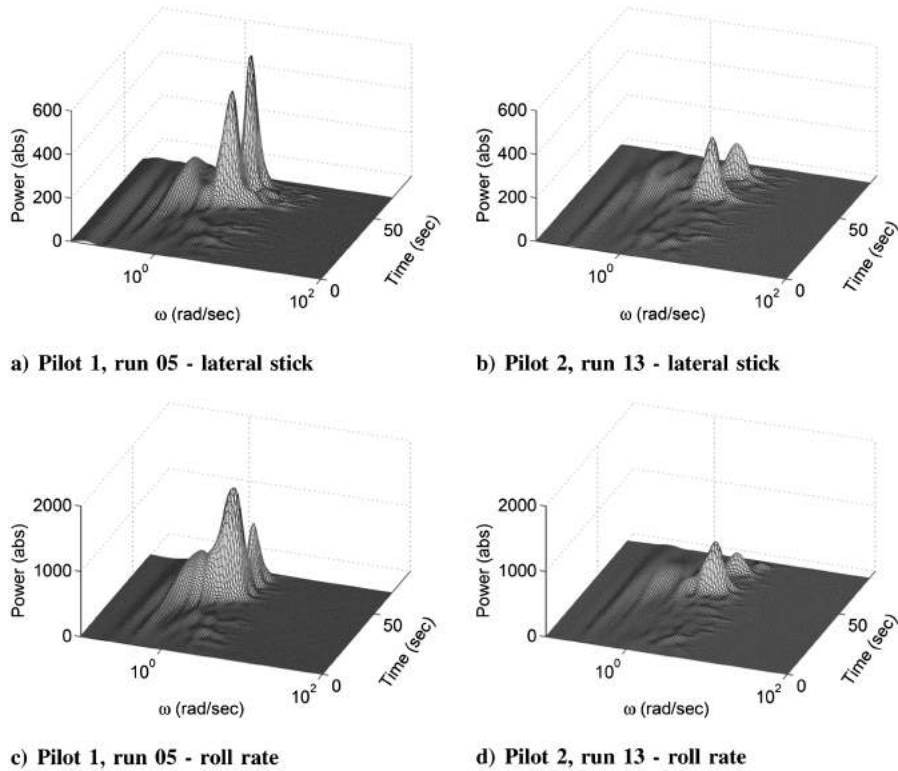


Fig. 9 Scalograms for pilot input and output in rate limited aircraft with no cuing.

in the early stages of the maneuver (the approach) and much activity in later stages (correction to centerline and landing). The main activity for both pilots is centered around the frequencies of 0.6–0.8 rad/s and 1.15 rad/s, which reflects characteristics from both of the previous cases. Unlike the rate-limited case, though, the magnitudes of the peaks are much more comparable to the baseline case. In effect, the scalograms directly exhibit the changes in the characteristics of pilot input and vehicle output behavior.

D. Time-Varying Cutoff and Power Frequency

One of the main challenges of scalograms is to draw some sort of quantitative meaning from them for comparison beyond the qualitative discussion like that in the previous section. The time-varying power frequency and the maximum power frequency are just such quantitative measures.

To better illustrate the motivation behind calculating the time-varying power frequency rather than just the time-varying cutoff

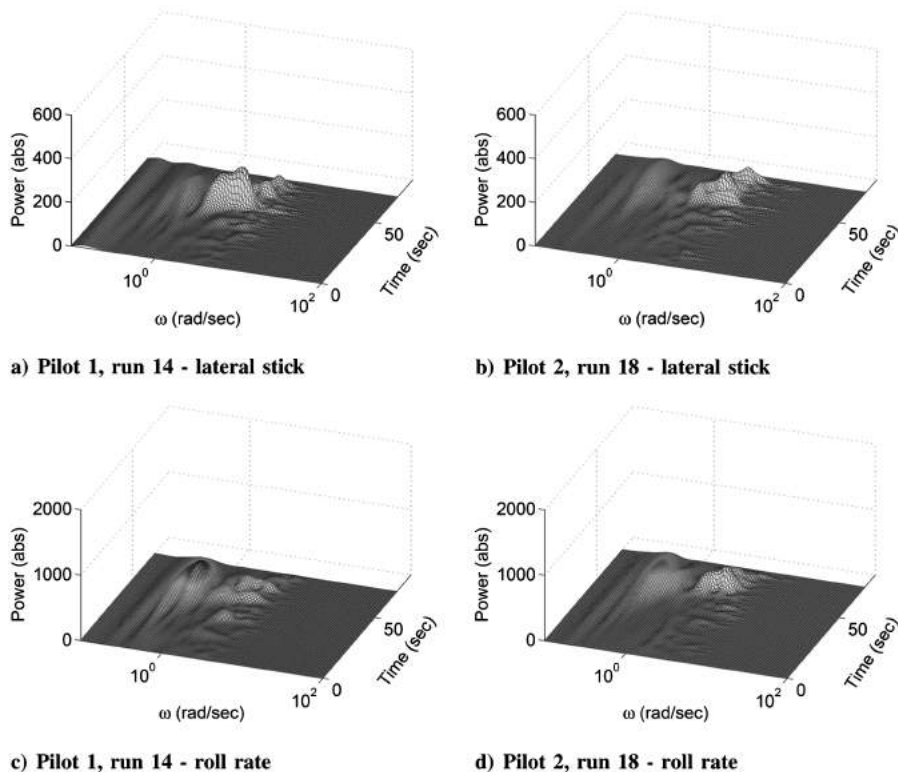


Fig. 10 Scalograms for pilot input and output in rate limited aircraft with cuing.

frequency, consider the time-varying cutoff frequencies (Fig. 11) for the example cases. For all of the cases, the cutoff frequency is generally the same magnitude regardless of aircraft configuration and the characteristics of their associated scalograms. There is little evidence in these figures of the changes in input and output power as the task progresses. However, they do reflect some of the subtle differences in pilot behavior. Recall that most of Pilot 1's input and output power were focused at particular frequencies and were of higher magnitude than that of Pilot 2. The differences in magnitude are not apparent in Fig. 11, but the difference in power distribution over the frequency range is. For all three aircraft configurations the cutoff frequency for Pilot 2 is generally higher than for Pilot 1. This means that Pilot 2, and subsequently the aircraft, exhibited more high frequency behavior, which is consistent with what was deduced from the scalograms.

Now consider the time-varying power frequencies for the example cases as shown in Fig. 12. The relative magnitude in power between pilots and aircraft configurations is readily visible in all four subfigures. The power frequency is quite low for the first 40 s of the run and then spikes, corresponding to the large pilot input and aircraft response in the time histories of Fig. 7 and the scalograms in Figs. 8–10 that is associated with the offset correction. The baseline cases have fairly low power frequencies, below 0.5 for pilot lateral stick input and below 1 for roll rate. The rate limited cases spike to almost 1.5 and 3.0 for Pilot 1 lateral stick input and roll rate, respectively, and to almost 0.75 and 2.0 for Pilot 2 lateral stick input and roll rate, respectively. The time-varying power frequency for the rate-limited with cueing cases returns to near baseline magnitude, but exhibits behavior similar to the rate-limited case.

E. Handling Qualities Rating vs. Power Frequency

The question now becomes 'Is the power frequency related to pilot handling qualities ratings?' If so, then the power frequency can be a beneficial addition to any analysis of a pilot-in-the-loop task because it will give an indication of the "goodness" or "badness" of an aircraft

configuration even without the pilot ratings. In the course of answering this question, two representative values of the power frequency are considered: the maximum power frequency determined from the scalogram-based time-varying power frequency and the average power frequency determined from the PSD of the overall run as generated by FREDa.

Tables 5 and 6 list the pilot ratings, maximum and average cutoff frequencies, and maximum and average power frequencies for the pilot input and vehicle output for each run, including the example cases. Some general trends that can be seen from these tables are that the maximum cutoff frequency for pilot lateral stick input tends to be larger than for aircraft roll rate and maximum power frequency for aircraft roll rate tends to be larger than pilot lateral stick input. The only exceptions to this trend are the maximum cutoff frequencies for Pilot 1 Run 6 and the maximum power frequencies for Pilot 1 Run 10 and 11. Conversely, average cutoff frequency for pilot lateral stick input tends to be less than for aircraft roll rate, and average power frequency for aircraft roll rate tends to be less than pilot lateral stick input.

A more informative way to visualize the data in these tables and assess the benefits of calculating the power frequency is to plot HQR versus the frequencies and determine if they are correlated. Figure 13 illustrates the frequency data as compared to the HQRs. Figures 13a and 13c show the maximum cutoff frequency data for both pilots. These data are scattered across the plots, and there is no obvious correlation between HQR and maximum cutoff frequency. The same can be said for average cutoff frequency as shown in Figs. 14a and 14c. These data are somewhat more clustered, but there is still no obvious correlation between HQR and average cutoff frequency.

Figures 13b and 13d tell a different story regarding the maximum power frequency. The data for both input and output exhibit an obvious correlation between HQR and maximum power frequency—HQR increases (i.e., handling qualities decreases) as maximum power frequency increases. Maximum power frequency

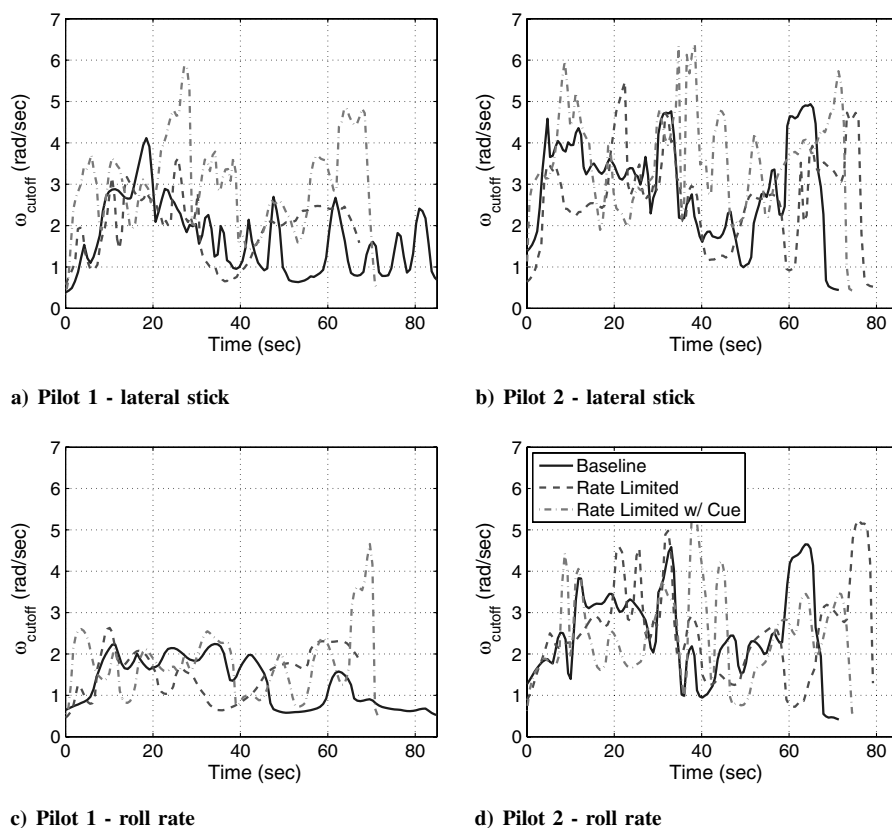


Fig. 11 Time-varying cutoff frequency for pilot input and output.

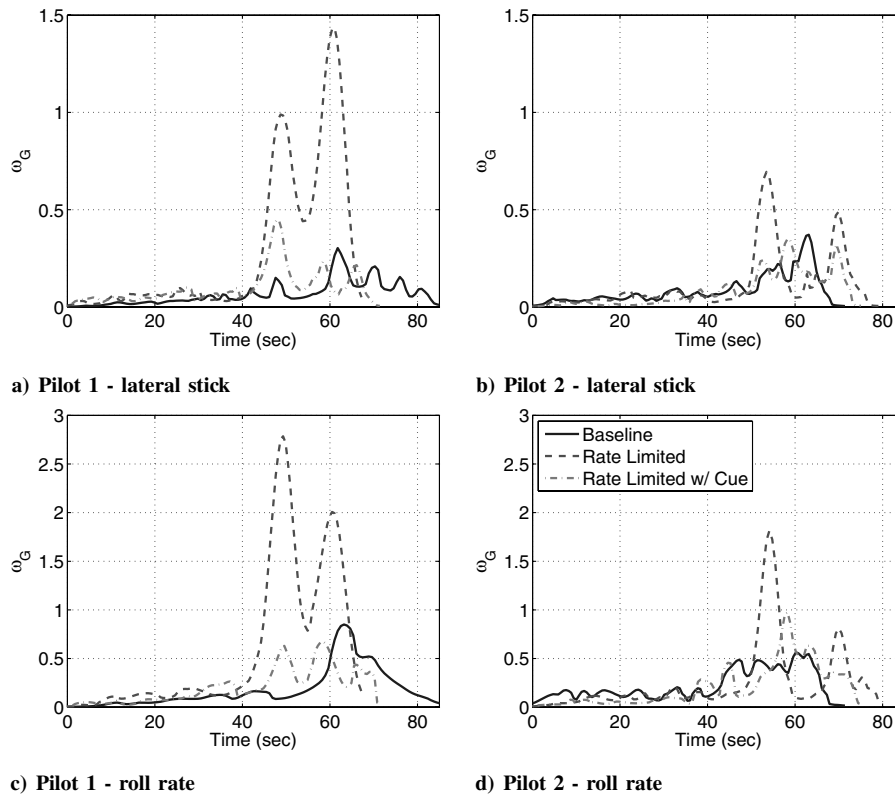


Fig. 12 Time-varying power frequency for pilot input and output.

and HQR are correlated more so for lateral stick input than for roll rate in which maximum power frequency ranges from 0.3 to 1.44, which are the baseline and rate-limited cases, respectively, for Pilot 1. The maximum power frequencies for the roll rate are somewhat more clumped between 0.5 and 1.5 with the rate-limited case outlier for

Pilot 1. Similarly, Figs. 14b and 14d illustrate a correlation between HQR and average power frequency. As for the maximum power frequency, HQR is directly proportional to average power frequency and increases as power frequency increases. There appears to be more scatter for the aircraft roll rate average power frequencies than

Table 5 Pilot 1 ratings and frequencies

Run	HQR	PIOR	$\omega_{\text{cutoff_max}}$		$\omega_{G_{\text{max}}}$		$\omega_{\text{cutoff_avg}}$		$\omega_{G_{\text{avg}}}$	
			Input	Output	Input	Output	Input	Output	Input	Output
04	3	1	4.11	2.24	0.30	0.85	1.47	0.92	0.10	0.19
05	10	5	3.63	2.63	1.44	2.78	2.25	1.74	0.54	0.76
06			4.32	5.31	0.74	0.76	2.23	1.82	0.23	0.29
07	5	3	4.47	3.72	0.54	0.95	2.56	1.82	0.13	0.24
08	8	4	5.77	3.46	0.62	0.86	3.07	2.22	0.31	0.57
09			5.64	4.79	0.67	0.99	2.84	2.54	0.23	0.29
10	8	4	4.95	4.83	0.99	0.94	2.15	2.05	0.32	0.38
11			5.87	4.40	0.61	0.61	2.41	1.90	0.11	0.24
12	4	2	5.96	3.23	0.40	0.42	2.54	1.18	0.11	0.15
13	8	4	6.11	5.16	1.37	0.97	2.77	2.08	0.25	0.25
14	4	2	5.86	4.66	0.45	0.68	2.76	1.71	0.10	0.22

Table 6 Pilot 2 ratings and frequencies

Run	HQR	PIOR	$\omega_{\text{cutoff_max}}$		$\omega_{G_{\text{max}}}$		$\omega_{\text{cutoff_avg}}$		$\omega_{G_{\text{avg}}}$	
			Input	Output	Input	Output	Input	Output	Input	Output
12	2	1	4.94	4.65	0.37	0.56	2.90	2.45	0.07	0.24
13	6	4	5.48	5.25	0.69	1.81	2.81	2.51	0.19	0.38
14	6	3	6.14	4.49	0.86	1.04	3.17	3.01	0.47	0.97
15	4	3	5.51	5.39	0.44	0.78	3.38	2.54	0.18	0.32
16	4	2	6.92	5.49	0.44	0.64	3.39	2.70	0.10	0.32
17			6.64	6.19	0.37	0.77	3.16	2.03	0.11	0.30
18	4	2	6.38	5.65	0.35	0.97	3.58	2.47	0.10	0.22
19	7	4	6.71	4.83	0.50	1.18	2.95	2.69	0.14	0.49

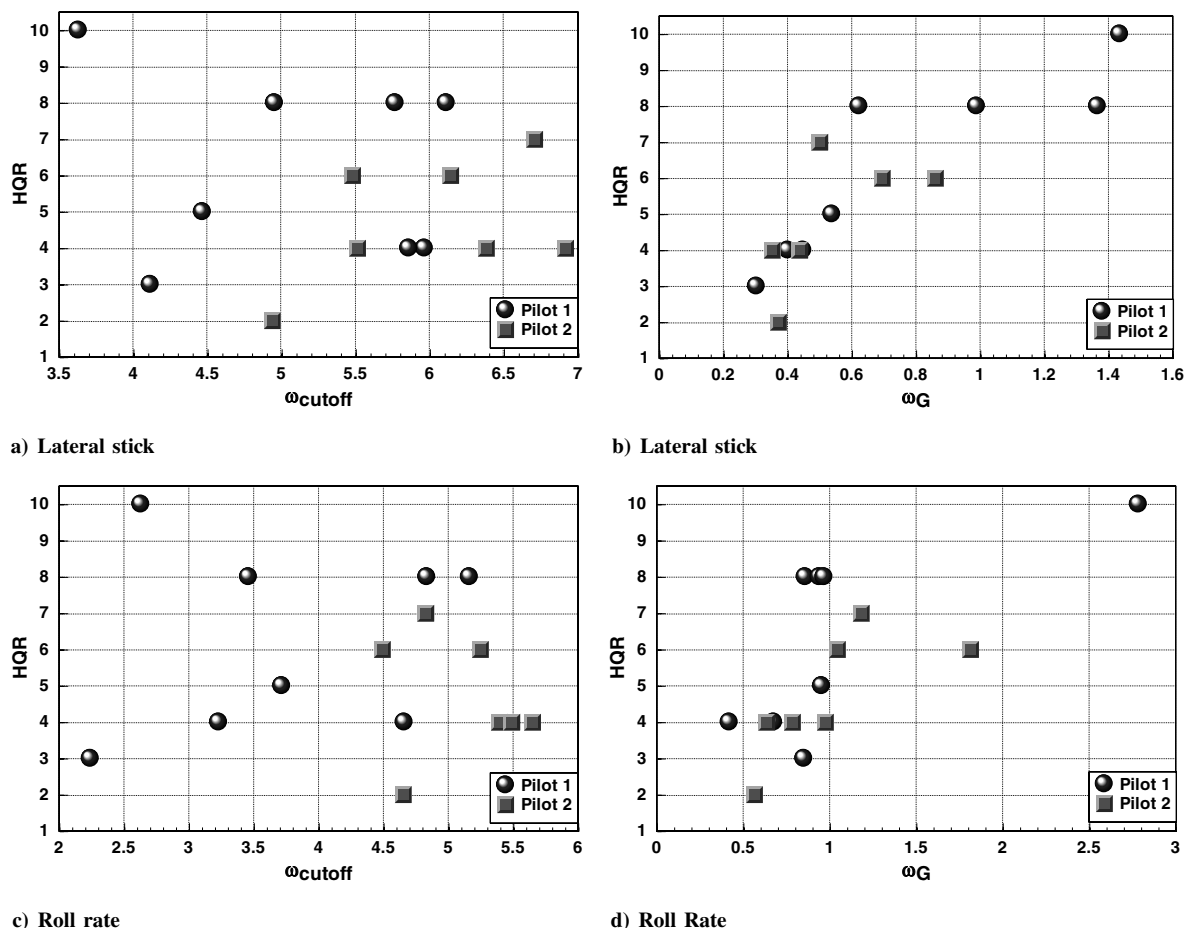


Fig. 13 Handling qualities ratings as a function of input/output maximum cutoff and power frequency.

for the maximum power frequency for both pilots. This is expected since HQR should reflect the effort required by the pilot to complete the task at hand, which translates to pilot input through the stick. In addition, greater pilot effort tends to translate to higher power reflected in the associated scalogram, which in turn leads to a higher maximum power frequency.

Aircraft roll rate does not necessarily respond in the same manner. The pilot could be expending great effort in an attempt to maneuver the aircraft, but the aircraft may be so under-actuated for one reason or another that it simply barely responds. This leads to little activity in the scalogram and thus a lower power frequency, yet the pilot rates the aircraft as Level 3. Therefore, there is some correlation between HQR and aircraft output and a much stronger correlation between HQR and pilot input.

Finally, consider the cases that were discussed in the previous sections: runs 04, 05, and 14 for Pilot 1 and runs 12, 13 and 18 for Pilot 2, representing baseline, rate-limited, and rate-limited with cuing cases, respectively. As listed in Table 5, Pilot 1 runs 04, 05, and 14 have HQRs 3, 10, and 4, maximum input power frequencies of 0.3, 1.44, and 0.45, and average input power frequencies of 0.10, 0.54, and 0.10. Table 6 lists the HQRs for Pilot 2 runs 12, 13, and 18 as 2, 6, and 4, maximum input power frequencies of 0.37, 0.69, and 0.35, and average input power frequencies of 0.07, 0.19, and 0.10. Between the two pilots there are similar trends. The baseline aircraft received Level 1 HQR and had maximum power frequencies around 0.3 and average power frequencies around 0.10. The rate-limited aircraft with cuing received barely Level 2 HQR with maximum input power frequency around 0.4 and average input power frequency of 0.10, which indicates a close return to nominal handling. The rate-limited case resulted in data that was not as consistent. Pilot 1 rated it as definitively Level 3 and had a high maximum input power frequency, but Pilot 2 rated it as on the high end of Level 2 and had a correspondingly lower maximum and average input power

frequency than Pilot 1. Possible reasons for this difference include basic differences in piloting technique and a comment by Pilot 2 saying he felt himself approach the “cliff” in the rate-limiting and backed off the task so as not encounter it.

In reference to Fig. 13b, the data for these example cases lie right along the trend in the data sets. The only two points that are a short distance from the maximum power frequency trend correspond to data for Pilot 1 Run 08 and Pilot 2 Run 19. There is only one point that can be claimed to be some distance from the average power frequency trend, and that is the data point for Pilot 2 Run 14. From Table 3, run 08 corresponds to rate-limited aircraft with a smart-gain that is slightly lower than all the other runs with cuing, which could account for the slight discrepancy. Table 3 lists run 14 as a rate-limited aircraft with smart-gain cuing only and run 19 as a rate-limited aircraft with no cuing. For run 14, it is possible the pilot did not care for or did not expect the effect of the smart-gain and fought the feedback. As for run 19, the pilot again backed off the task as he approached the cliff in rate-limiting and thus had a fairly low maximum input power frequency, but in this case he rated the aircraft as Level 3 instead of Level 2 as he did in run 13. This small difference is an expected amount of variation in such a rating scheme.

F. Discussion

This initial development and analysis of the power frequency shows promise as a new pilot-vehicle system response analysis metric. The investigation presented herein was limited in data analyzed and scope to facilitate the development of the metric. To confirm the results and better solidify the conclusions drawn, a more extensive analysis using multiple aircraft, pilots, and tasks is necessary. However, these initial results are encouraging that the power frequency can be a useful addition to the pilot-vehicle analysis regime.

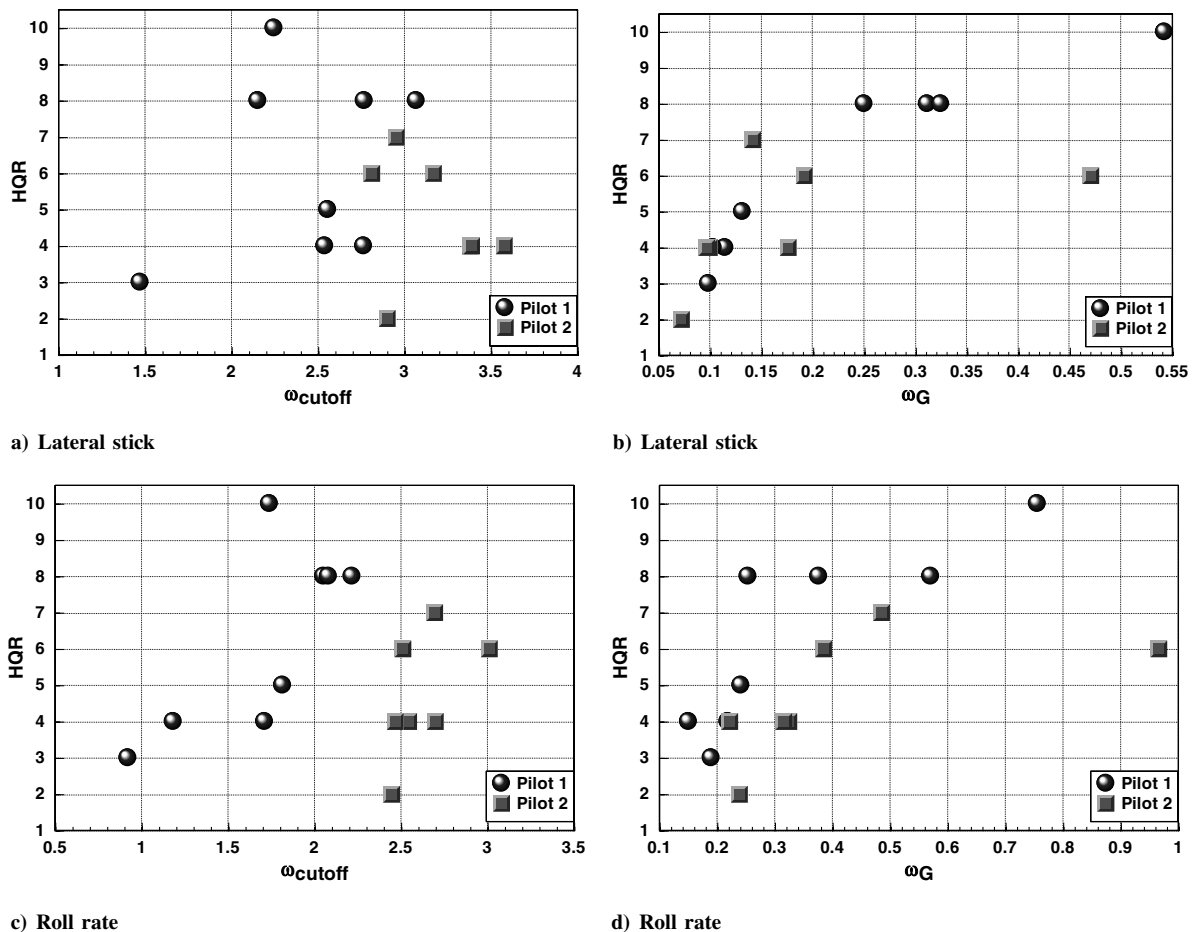


Fig. 14 Handling qualities ratings as a function of input/output average cutoff and power frequency.

VI. Conclusions

A flight test study that was conducted using the Calspan Learjet in-flight simulator as a means to explore various combinations of inceptor cueing and command path gain adjustment in the presence of actuator rate-limiting was used to assess the utility of a new metric, the power frequency, for pilot-in-the-loop tasks that do not lend themselves to calculation of crossover frequency. The results of this study point to several conclusions derived from the power frequency analysis.

The time-varying power frequency and maximum power frequency provides a promising new means to analyze pilot-vehicle system responses for pilot-in-the-loop tasks in addition to those metrics already utilized by the handling qualities community. The dependence of time-varying power frequency on both the magnitude of the power spectra density and the distribution of the power over the frequency separates it from time-varying cutoff frequency, which is only dependent on power distribution over the frequency and does not reflect the relative effort of the pilot and response of the aircraft as the task progresses. Handling qualities rating and maximum power frequency are directly correlated, especially for pilot input power. This correlation is dependent on the consistency of the pilot who is rating the task, but this correlation suggests that maximum input power frequency is an indicator of the effort required by the pilot to complete a task. For the flight data analyzed, time-varying cutoff frequency and maximum cutoff frequency show little to no correlation with handling qualities rating and do not reflect the changes in power magnitude evident in the scalograms. They do show changes in power distribution over the frequency range, which could prove to be useful after more in depth analysis.

References

- [1] Cooper, G. E., Robert, P., and Harper, J., "The Use of Pilot Rating in the Evaluation of Aircraft Handling Qualities," National Aeronautics and Space Administration, TR NASA TN D-5153, Apr. 1969.
- [2] DiFranco, D. A., "Flight Investigation of Longitudinal Short Period Frequency Requirements and PIO Tendencies," Air Force Flight Dynamics Lab., TR AFFDL-TR-66-163, June 1967.
- [3] Dept. of Defense, "Flying Qualities of Piloted Aircraft," MIL TR STD-1797B, 15 Feb. 2006.
- [4] Baskett, B. J., "Aeronautical Design Standard, Performance Specification: Handling Qualities Requirements for Military Rotorcraft," U.S. Army Aviation and Missile Command TR ADS-33E-PRF, U.S. Army Aviation and Missile Command, Redstone Arsenal, AL, Mar. 2000.
- [5] Mitchell, D. G., Doman, D. B., Key, D. L., Klyde, D. H., Leggett, D. B., Moorhouse, D. J., Mason, D. H., Raney, D. L., and Schmidt, D. K., "Evolution, Revolution, and Challenges of Handling Qualities," *Journal of Guidance, Control, and Dynamics*, Vol. 27, No. 1, Jan.–Feb. 2004, pp. 12–28. doi:10.2514/1.3252
- [6] Wunnenberg, H., "Handling Qualities of Unstable Highly Augmented Aircraft," AGARD No. AR-279, Jan. 1991.
- [7] McRuer, D. T., and Krendel, E. S., "Mathematical Models of Human Pilot Behavior," AGARDograph No. 188, Nov. 1973.
- [8] Tischler, M. B., and Remple, R. K., *Aircraft and Rotorcraft System Identification: Engineering Methods and Flight Test Examples*, AIAA Education Series, American Institute of Aeronautics and Astronautics, Reston, VA, 2006.
- [9] Lawrence, B., Malpica, C. A., Theodore, C. R., Decker, W. A., and Lindsey, J. E., "Flight Dynamics Aspects of a Large Civil Tiltrotor Simulation Using Translational Rate Command," *American Helicopter Society 67th Annual Forum*, American Helicopter Society, Virginia Beach, VA, 3–5 May 2011.
- [10] Klyde, D. H., Bachelder, E. N., McMahon, R., Weingarten, N. C., and Harris, C., "Use of In-Flight Simulation to Create a Flying Qualities Database," U.S. Air Force T&E Days, AIAA Paper 2008-1624, Los Angeles, CA, 5–7 Feb. 2008.
- [11] Deppe, P. R., Chalk, C. R., and Shafer, M. F., "Flight Evaluation of an Aircraft with Side and Center Stick Controllers and Rate-Limited Ailerons," National Aeronautics and Space Administration, TR NASA

- CR-198055, Nov. 1996.
- [12] Klyde, D. H., and McRuer, D., "Development of Smart-Cue and Smart-Gain Concepts to Alleviate Pilot-Vehicle System Loss of Control," *Journal of Guidance, Control, and Dynamics*, Vol. 32, No. 5, Sept.–Oct. 2009, pp. 1409–1417.
doi:10.2514/1.43156
- [13] Klyde, D. H., and Liang, C. Y., "Approach and Landing Flight Test Evaluation of Smart-Cue and Smart-Gain Concepts," *Journal of Guidance, Control, and Dynamics*, Vol. 32, No. 4, July–Aug. 2009, pp. 1057–1070.
doi:10.2514/1.43157
- [14] Atencio, A., Jr., "Fidelity Assessment of a UH-60A Simulation on the NASA Ames Vertical Motion Simulator," National Aeronautics and Space Administration, TR NASA TM 104016, Sept. 1993.
- [15] McRuer, D. T., and Krendel, E. S., "Mathematical Models of Human Pilot Behavior," Advisory Group for Aerospace Research and Development, AGARDograph TR No. 188, Nov. 1973.
- [16] Myers, T. T., Aponso, B. L., Klyde, D. H., Rosenthal, T. J., and Magdaleno, R. E., "FREDA—Frequency Domain Analysis Program User's Guide," Systems Technology, Inc., TR STI-WP-0433-02, Hawthorne, CA, 1988.
- [17] Klyde, D. H., Shulze, P. C., Thompson, P. M., and Liang, C. Y., "Use of Wavelet Scalograms to Characterize Rotorcraft Pilot-Vehicle System Interactions," *American Helicopter Society 66th Annual Forum*, American Helicopter Society, Phoenix, AZ, 11–13 May 2010.

J. Valasek
Associate Editor